




A Kalman filter application for rainfall estimation using radar reflectivity measurements

Engin MAŞAZADE^{1,*}, Ali Kemal BAKIR^{2,3}, Pınar KIRCI³

¹Department of Electrical & Electronics Engineering, Faculty of Engineering, Yeditepe University, İstanbul, Turkey

²Turkish State Meteorological Service, Kocaeli, Turkey

³Department of Engineering Sciences, Faculty of Engineering, İstanbul University, İstanbul, Turkey

Received: 01.08.2018

Accepted/Published Online: 17.12.2018

Final Version: 22.03.2019

Abstract: The rainfall amount observed at a given location mostly depend on the cloud density, which can be quantified with the reflectivity values observed by meteorology weather radars. In this study, we aim to estimate the rainfall amount using a Kalman filter with radar reflectivity measurements. We first assume that the amount of rainfall observed at automatic weather observation stations (AWOSs) are elements of an unknown state vector and consider the Kalman filter process model as the true rainfall amounts observed at these AWOSs over time. For the measurement model of the Kalman filter, we use the radar reflectivity values observed at each AWOS location. For the execution of the Kalman filter, a number of rainfall amount and radar reflectivity value pairs are first required to learn the process and measurement models of the Kalman filter. The estimation performance of the proposed Kalman filter is then compared with empirical reflectivity (Z) - rainfall (R) relationships. Numerical results show that when the Kalman filter is executed with radar reflectivity measurements observed around a large number of AWOS locations, the mean squared errors of the Kalman filter rainfall estimates are smaller than the ones obtained with empirical ZR relationships.

Key words: Kalman filter, multivariate least squares, radar reflectivity measurements, rainfall estimation

1. Introduction

Weather forecasting predicts the level of precipitation, cloudiness, temperature, wind speed, and direction for a given time period in the near future. Short-time forecasting refers to the determination of the weather conditions for the next 12 h; on the other hand, nowcasting refers to determination of the weather activity for the next 6 h. Nowcasting is critical to warn the public about severe weather that may have a harsh effect on social life and economic activities. As an example, an early warning about severe weather is important to reduce disaster risks.

Meteorology weather radar, also called weather surveillance radar (WSR) or Doppler weather radar, is a type of radar used to locate precipitation, calculate its motion, and estimate its type such as rain, snow, or hail. Return echoes from clouds, called reflectivity measurements, are then analyzed for their intensities to establish the precipitation rate in the scanned volume. The radar reflectivity values, Z (or dBZ in its decibel scale), increase with the severity of the pulse returns where stronger returns may indicate not only heavy rain but also thunderstorms or hail [1]. There is an empirical relationship between radar reflectivity value Z in millimeters to the sixth power per cubic meter (mm^6/mm^3) and the corresponding rainfall amount R in millimeters per

*Correspondence: engin.masazade@yeditepe.edu.tr

hour (*mm/hour*) as $Z = aR^b$, where the empirical ZR relationship parameters a and b vary based on the type of the rainfall [2-6].

One branch of research is interested in tracking the cloud activity, which employs spatial or temporal interpolation between consecutively observed radar reflectivity measurements (see [7] and references therein). However, in this work, our aim is to directly predict the amount of rainfall at each automatic weather observation station (AWOS) based on the radar reflectivity measurements. The ZR relationship parameters a and b depend on the type of the rainfall [5] and may change over time [6]. Additionally, there might be some bias between the predicted and the true rainfall amount, which may require further calibration [5]. A logarithmic bias model between the predicted and the true rainfall amount was presented in [8, 9], where the authors additionally employed a Kalman filter [10] to estimate the bias term over time. Additional bias models, linear and power law models, were also given in [11]. Then the authors of [12] first determined the optimal parameters of the ZR relationship for given weather data and compared their precipitation estimates with the Kalman filter used for bias correction. For the Kalman filter, the process and measurement model parameters need to be determined first. The works presented in [9, 11] model the bias value over time as an autoregressive-one (AR(1)) model. For bias correction in rainfall estimation, in [9], Kalman filter model parameters were obtained by trial and error. In [11], Kalman filter model parameters were estimated by using nonparametric estimators based on the method of moments, which does not assume any distribution for the errors.

In this work, we are interested in estimating the precipitation amount for nowcasting. Rather than using the conventional empirical ZR relationships, our aim is to predict the rainfall amount at a given AWOS location by not only considering the current and previously received radar reflectivity measurements only around that location, but also including the current and previously received radar reflectivity measurements around the neighboring AWOS locations. Note that in order to predict the rainfall amount at a given AWOS location, our method does not need the observed rainfall amounts in the previous steps of tracking. Here, rather than forming an AR(1) model, we form a vector autoregressive-one VAR(1) model [13] where elements of the state vector represent the true but unknown rainfall amounts observed at different AWOS locations. In our work, the parameters of the process and measurement models of the Kalman filter are determined by using multivariate least squares, which requires some initial training data consisting of radar reflectivity measurements and rainfall amount data pairs. Numerical results show that as we increase the number of participating AWOS locations to estimate the rainfall amount at a given location, Kalman filter predictions significantly outperform the predictions generated with the empirical ZR relationships.

The rest of the paper is organized as follows. In Section 2, we give a brief review of meteorology radars and the relationship between rainfall predictions and radar reflectivity measurements. In Section 3, we present the Kalman filter model, determination of the Kalman filter model parameters, and execution of the Kalman filter. In Section 4, we present the numerical results, and finally in Section 5, we conclude the paper and address fruitful research directions.

2. Rainfall prediction from radar reflectivity measurements

Modern weather radars are typically pulse-Doppler radars, which can detect both the motion of rain droplets and the precipitation intensity. Both types of data are then analyzed to determine the structure of weather activity and their potential to cause severity. Weather radars send directional pulses on the order of 1 ms long. Between each pulse, the radar serves as a receiver and listens for return signals from particles in the air. The listen cycle duration is on the order of 1 ms, which is about 1000 times longer than the pulse duration. The

typical values of equivalent radar reflectivity measurements from different types of weather activities (targets) are shown in Table 1.

Table 1. The typical values of equivalent radar reflectivity values from different targets [1].

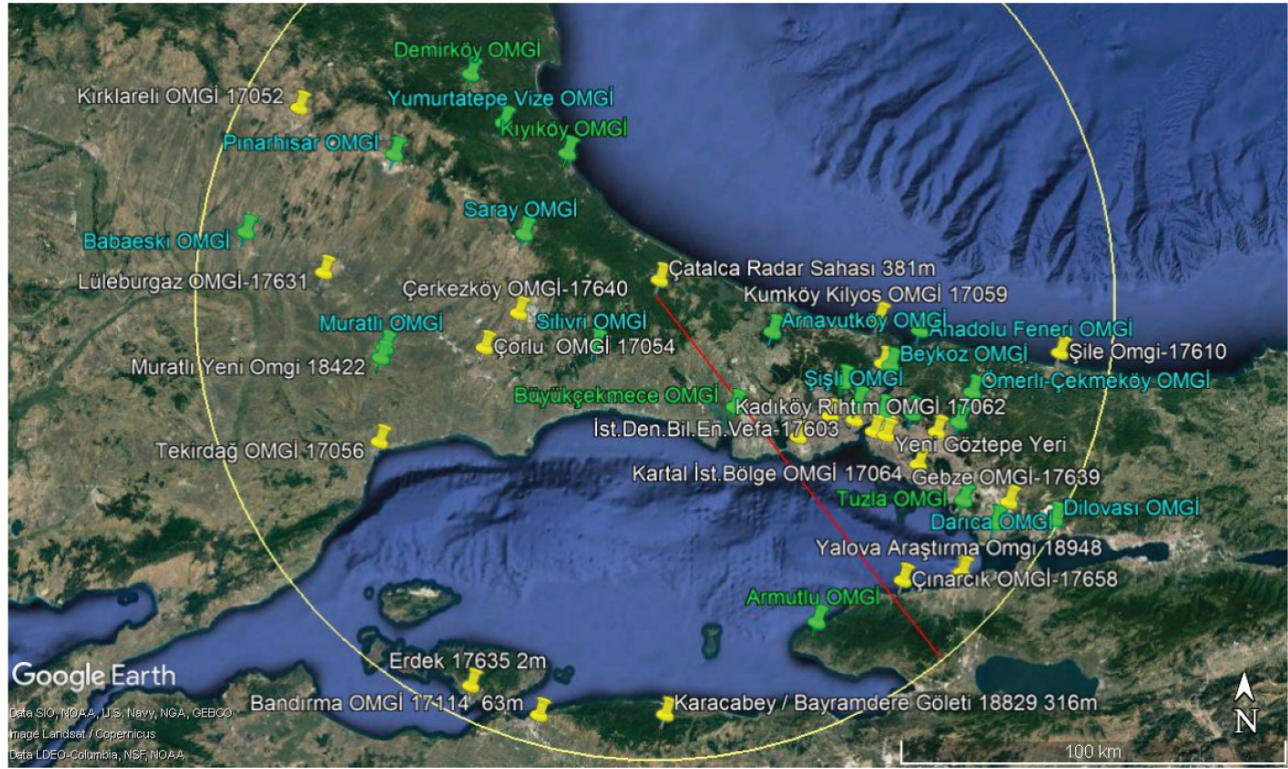
Target	Z , (dBZ)
Light drizzle	0
Moderate drizzle, light snow	10
Light rain or moderate snow	25
Moderate rain	35
Heavy rain	45
Hail or very heavy rain	55
Moderate or severe hail	> 60

Z–R relationships map the radar reflectivity measurements (Z) into rainfall amount predictions (R) for the types of precipitation as shown in Table 2. As an example, the precipitation generated by warm rain processes such as drizzle results in smaller drops and has climatological Z–R relationships with smaller a coefficients (a weaker reflectivity will be observed for the same rain rate because of the smaller drops). Examples of other Z–R relationships include the Marshall–Palmer Z–R relationship $Z = 200R^{1.6}$, suitable for stratiform precipitations [3, 14], or the relationship applicable to convective precipitation $Z = 300R^{1.4}$, which is widely used by the US National Weather Service (NWS) [1, 4, 15, 16]. There are many criteria that may be used to separate stratiform precipitation from the convective one [1, 17, 18]. First of all, the type of cloudiness, such as cumuliform types, may characterize convective air and convective precipitation. A convective air mass is rapid and efficient. When compared with stratiform precipitation, convective precipitation is unstable and has vertical air motions within clouds. Particles in convective precipitation drift both upwards and downwards, while particles mostly drift downward in stratiform precipitation [17]. On the other hand, stratiform precipitation may also have small cells of convection [1]. At usual weather radar wavelengths, strong echoes (>40 dBZ) originate from convective precipitation, and the strongest echoes (> 60 dBZ) are generally associated with hail. Stratiform precipitations, on the other hand, do not have peak echoes above 40 dBZ.

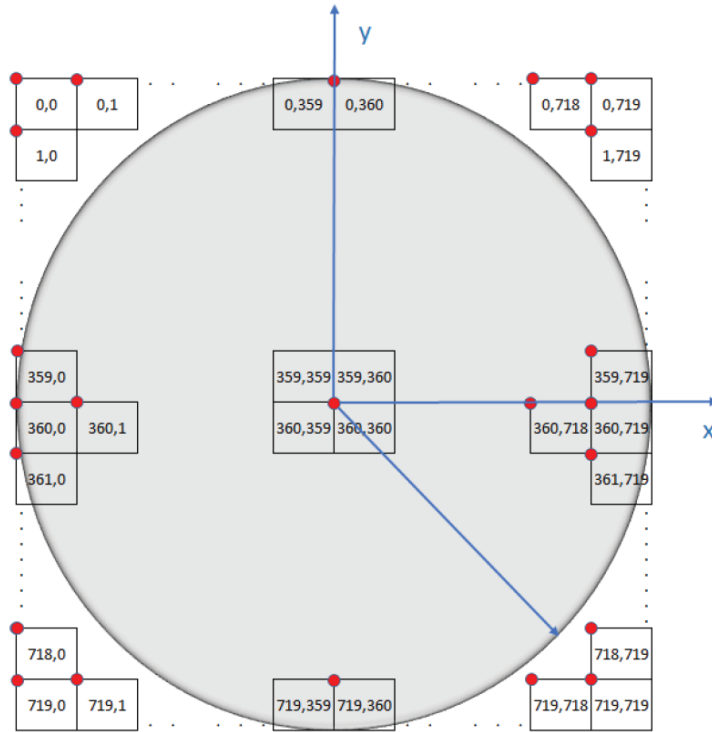
Table 2. The empirical relationship between reflectivity and rainfall for different precipitation types [3, 4].

Empirical Z-R relationship	Rain type
$Z = 140R^{1.5}$	Light drizzle
$Z = 200R^{1.6}$	Stratiform precipitation
$Z = 300R^{1.4}$	Convective precipitation

In this work, we obtain the radar reflectivity data from the Çatalca radar in Turkey, whose location is shown in Figure 1a. The Çatalca radar is owned and operated by the Turkish State Meteorological Service. The Çatalca radar is a C-band Doppler radar that transmits radiation with a wavelength of 5.33 cm and produces a beam-width of 0.56 degrees. The radar reflectivity measurements have been derived from the 1-km constant altitude plan position indicator (CAPPI) data spanning an area with a radius of 120 km from the radar location. CAPPI radar reflectivity data have been provided in a Cartesian grid, as shown in Figure 1b, of 720×720 with



(a)



(b)

Figure 1. (a) Çatalca radar observation range and locations of the AWOSs, (b) radar coverage region partitioned into pixels.

about 0.11 km^2 spatial resolution for each pixel and 8 min of temporal resolution. In a Cartesian grid, the radar is located in the upper left corner of the pixel (360,360), which represents the center of the disk having a radius of 120 km. Within the range of the Çatalca radar, there are a number of automatic weather observation stations (AWOS), where an AWOS is equipped with sensors that can measure meteorological parameters such as precipitation, temperature, wind speed, and wind direction. Radar reflectivity and rain gauge data around a particular AWOS location need to be recorded at the same time for this study.

In this work, we are interested in predicting rainfall amounts of up to $N = 15$ AWOSs having rain gauge sensors located in the southern part of İstanbul Province as shown in Figure 2. The locations of the AWOSs of interest are also given in Table 3 in terms of their pixel values within the range of the Çatalca radar. The Turkish State Meteorological Service (TSMS) is a founder state of the World Meteorological Organization, the WMO being responsible to make regulations in the meteorological area, such as measurements, instrumentation, observations, nowcasting, etc. In our work, we are interested in precipitation measurements on the ground. The WMO suggests that the location of precipitation stations within the area of interest is important, because the number and locations of the rain gauge sites should determine how well the rain gauge observations represent the actual amount of precipitation falling in the area. Therefore, the rainfall parameter should be considered as the area average. In order to express the radar reflectivity over the same area and to associate it with the rain gauge rainfall amount for each AWOS location, we average the radar reflectivity values over 25 pixels of CAPPI data, where the AWOS is located at the center of these 25 pixels [19].

Table 3. Automatic weather observation stations (AWOSs) used in this work within the range of the Çatalca radar.

Sensor no.	AWOS name	Pixel value	Sensor no.	AWOS name	Pixel value
S_1	Şişli	(455,513)	S_9	Kartal	(503,560)
S_2	Kadiköy	(477,526)	S_{10}	Tuzla	(531,595)
S_3	Ümraniye	(463,556)	S_{11}	Büyükkçekmece	(458,418)
S_4	Sancaktepe	(470,529)	S_{12}	Davutpaşa	(424,534)
S_5	Darica	(549,619)	S_{13}	Vefa	(468,511)
S_6	Florya	(481,467)	S_{14}	Eyüp	(439,502)
S_7	Üsküdar	(462,533)	S_{15}	Sarıyer	(424,534)
S_8	Samandıra	(478,575)			

3. Kalman filter for rainfall estimation

In this section we briefly review the properties of the Kalman filter [10]. We then review the multivariate least squares method, which is used for estimating the process and measurement models of the Kalman filter. We finally relate the prediction and update models of the Kalman filter according to the rainfall estimation problem.

3.1. Kalman filter model

Let \mathbf{x}_t represent the true state vector of size $N \times 1$ at time step t . The true state at time t evolves from the previous state $t - 1$ according to the process model as

$$\mathbf{x}_t = \mathbf{F}\mathbf{x}_{t-1} + \mathbf{w}_t, \quad (1)$$



Figure 2. Locations of the AWOSs having rain gauge sensors.

where \mathbf{F} is the $N \times N$ state transition matrix applied to the previous state \mathbf{x}_{t-1} , and \mathbf{w}_t is the process noise, which is assumed to be drawn from a zero mean multivariate Gaussian distribution with covariance matrix \mathbf{Q} of size $N \times N$.

At time step t , a measurement vector \mathbf{z}_t of size $M \times 1$ is obtained from the true state \mathbf{x}_t according to the measurement model as

$$\mathbf{z}_t = \mathbf{H}\mathbf{x}_t + \mathbf{v}_t, \quad (2)$$

where \mathbf{H} is the measurement matrix of size $M \times N$, which maps the true state space into measurement space, and \mathbf{v}_t is the zero mean multivariate Gaussian measurement noise with covariance matrix \mathbf{R} of size $M \times M$.

In our problem formulation, \mathbf{x}_t represents the amount of rain collected in N different AWOS rain gauge sensors located in a given region of interest. In this problem, our task is to estimate the amount of rain $\hat{\mathbf{x}}_{t|t}$ at each time step t , using the radar reflectivity measurements \mathbf{z}_t . In this work, $M = N$, where the size of the radar reflectivity measurement vector M becomes equal to the size of the unknown state N , i.e. the true rainfall amounts observed at the AWOS locations where the radar reflectivity measurements have also been taken.

3.2. Kalman filter model estimation

Let us have the observation pair $(\mathbf{x}_t, \mathbf{z}_t)$ for $t \in \{1, 2, \dots, T\}$, where T represents the total number of pairs used for training, i.e. Kalman filter model estimation. Let the actual rainfall information for T steps of tracking be $\mathbf{x}_1, \dots, \mathbf{x}_T$ (where $\mathbf{x}_t = [x_{1,t}, x_{2,t}, \dots, x_{N,t}]^T$ and $x_{i,t}$ represents the true rainfall amount observed at the

i th AWOS rain gauge sensor at time step t) obeying a vector autoregression model, VAR(1), as follows:

$$\underbrace{\begin{pmatrix} x_{1,t} \\ x_{2,t} \\ \vdots \\ x_{N,t} \end{pmatrix}}_{\mathbf{x}_t} = \underbrace{\begin{pmatrix} a_{1,1} & a_{1,2} & \cdots & a_{1,N} \\ a_{2,1} & a_{2,2} & \cdots & a_{2,N} \\ \vdots & \vdots & \ddots & \vdots \\ a_{N,1} & a_{N,2} & \cdots & a_{N,N} \end{pmatrix}}_{\mathbf{F}} \underbrace{\begin{pmatrix} x_{1,t-1} \\ x_{2,t-1} \\ \vdots \\ x_{N,t-1} \end{pmatrix}}_{\mathbf{x}_{t-1}} + \underbrace{\begin{pmatrix} w_{1,t} \\ w_{2,t} \\ \vdots \\ w_{N,t} \end{pmatrix}}_{\mathbf{w}_t} \quad t \in \{2, \dots, T\}. \quad (3)$$

The above VAR(1) includes $T - 1$ recursions, and all recursions can be written in a compact form as

$$\mathbf{Y}_1 = \mathbf{B}_1 \mathbf{Z}_1 + \mathbf{U}_1, \quad (4)$$

where $\mathbf{Y}_1 = \begin{pmatrix} x_{1,2} & x_{1,3} & \cdots & x_{1,T} \\ x_{2,2} & x_{2,3} & \cdots & x_{2,T} \\ \vdots & \vdots & \ddots & \vdots \\ x_{N,2} & x_{N,3} & \cdots & x_{N,T} \end{pmatrix}$, $\mathbf{B}_1 = \begin{pmatrix} a_{1,1} & a_{1,2} & \cdots & a_{1,N} \\ a_{2,1} & a_{2,2} & \cdots & a_{2,N} \\ \vdots & \vdots & \ddots & \vdots \\ a_{N,1} & a_{N,2} & \cdots & a_{N,N} \end{pmatrix}$, $\mathbf{Z}_1 = \begin{pmatrix} x_{1,1} & x_{1,2} & \cdots & x_{1,T-1} \\ x_{2,1} & x_{2,2} & \cdots & x_{2,T-1} \\ \vdots & \vdots & \ddots & \vdots \\ x_{N,1} & x_{N,2} & \cdots & x_{N,T-1} \end{pmatrix}$,
 and $\mathbf{U}_1 = \begin{pmatrix} w_{1,2} & w_{1,3} & \cdots & w_{1,T} \\ w_{2,2} & w_{2,3} & \cdots & w_{2,T} \\ \vdots & \vdots & \ddots & \vdots \\ w_{N,2} & w_{N,3} & \cdots & w_{N,T} \end{pmatrix}$. From Eq. (4), the multivariate least squares estimate of \mathbf{B}_1 , $\hat{\mathbf{B}}_1$, is

obtained as [13]

$$\hat{\mathbf{B}}_1 = \mathbf{Y}_1 \mathbf{Z}_1^T (\mathbf{Z}_1 \mathbf{Z}_1^T)^{-1} \quad (5)$$

and the error covariance matrix is estimated as [13]

$$\hat{\Sigma}_1 = \frac{(\mathbf{Y}_1 - \hat{\mathbf{B}}_1 \mathbf{Z}_1)(\mathbf{Y}_1 - \hat{\mathbf{B}}_1 \mathbf{Z}_1)^T}{(T - 1) - N - 1}, \quad (6)$$

where the normalization factor $(T - 1) - N - 1$ ensures that $\hat{\Sigma}_1$ is an unbiased estimate of the true but unknown error covariance matrix Σ_1 . Then, in Eq. (1), we set the process model matrix $\mathbf{F} = \hat{\mathbf{B}}_1$ and process noise covariance matrix $\mathbf{Q} = \hat{\Sigma}_1$.

We use the actual rainfall values, $\mathbf{x}_1, \dots, \mathbf{x}_T$, and their corresponding radar reflectivity measurements, $\mathbf{z}_1, \dots, \mathbf{z}_T$, up to time step T as follows:

$$\underbrace{\begin{pmatrix} z_{1,t} \\ z_{2,t} \\ \vdots \\ z_{N,t} \end{pmatrix}}_{\mathbf{z}_t} = \underbrace{\begin{pmatrix} b_{1,1} & b_{1,2} & \cdots & b_{1,N} \\ b_{2,1} & b_{2,2} & \cdots & b_{2,N} \\ \vdots & \vdots & \ddots & \vdots \\ b_{N,1} & b_{N,2} & \cdots & b_{N,N} \end{pmatrix}}_{\mathbf{H}} \underbrace{\begin{pmatrix} x_{1,t} \\ x_{2,t} \\ \vdots \\ x_{N,t} \end{pmatrix}}_{\mathbf{x}_t} + \underbrace{\begin{pmatrix} v_{1,t} \\ v_{2,t} \\ \vdots \\ v_{N,t} \end{pmatrix}}_{\mathbf{v}_t} \quad t \in \{1, \dots, T\}. \quad (7)$$

Similar to Eq. (4), we can represent all T radar reflectivity and corresponding rainfall amount pairs in a compact form as

$$\mathbf{Y}_2 = \mathbf{B}_2 \mathbf{Z}_2 + \mathbf{U}_2, \quad (8)$$

$$\text{where } \mathbf{Y}_2 = \begin{pmatrix} z_{1,1} & z_{1,2} & \cdots & z_{1,T} \\ z_{2,1} & z_{2,2} & \cdots & z_{2,T} \\ \vdots & \vdots & \ddots & \vdots \\ z_{N,1} & z_{N,2} & \cdots & z_{N,T} \end{pmatrix}, \mathbf{B}_2 = \begin{pmatrix} b_{1,1} & b_{1,2} & \cdots & b_{1,N} \\ b_{2,1} & b_{2,2} & \cdots & b_{2,N} \\ \vdots & \vdots & \ddots & \vdots \\ b_{N,1} & b_{N,2} & \cdots & b_{N,N} \end{pmatrix}, \mathbf{Z}_2 = \begin{pmatrix} x_{1,1} & x_{1,2} & \cdots & x_{1,T} \\ x_{2,1} & x_{2,2} & \cdots & x_{2,T} \\ \vdots & \vdots & \ddots & \vdots \\ x_{N,1} & x_{N,2} & \cdots & x_{N,T} \end{pmatrix},$$

$$\text{and } \mathbf{U}_2 = \begin{pmatrix} v_{1,1} & v_{1,2} & \cdots & v_{1,T} \\ v_{2,1} & v_{2,2} & \cdots & v_{2,T} \\ \vdots & \vdots & \ddots & \vdots \\ v_{N,1} & v_{N,2} & \cdots & v_{N,T} \end{pmatrix}. \text{ Then the multivariate least squares estimate of } \mathbf{B}_2, \hat{\mathbf{B}}_2, \text{ is obtained as}$$

$$\hat{\mathbf{B}}_2 = \mathbf{Y}_2 \mathbf{Z}_2^T (\mathbf{Z}_2 \mathbf{Z}_2^T)^{-1} \quad (9)$$

and the unbiased covariance matrix estimate of the measurement noise becomes

$$\hat{\mathbf{\Sigma}}_2 = \frac{(\mathbf{Y}_2 - \hat{\mathbf{B}}_2 \mathbf{Z}_2)(\mathbf{Y}_2 - \hat{\mathbf{B}}_2 \mathbf{Z}_2)^T}{T - N - 1}. \quad (10)$$

Finally, in Eq. (2), we set the measurement model matrix $\mathbf{H} = \hat{\mathbf{B}}_2$ and measurement noise covariance matrix $\mathbf{R} = \hat{\mathbf{\Sigma}}_2$.

3.3. Execution of the Kalman filter

The Kalman filter is a recursive estimator; that is, only the estimated state from the previous time step and the current measurement are needed to compute the estimate for the current state. Let $\hat{\mathbf{x}}_{t|t}$ represent the a posteriori state estimate at time t given observations up to and including time step t and let $\mathbf{P}_{t|t}$ be the a posteriori error covariance matrix. Then the Kalman filter is implemented in two distinct stages as prediction and update [10].

During the prediction stage, for time step t , the predicted a priori state estimate, $\hat{\mathbf{x}}_{t|t-1}$, and a priori error covariance matrix, $\mathbf{P}_{t|t-1}$, are respectively obtained from the a posteriori state estimate $\hat{\mathbf{x}}_{t-1|t-1}$ and a posteriori error covariance matrix $\mathbf{P}_{t-1|t-1}$ of the previous time step $t-1$ as

$$\begin{aligned} \hat{\mathbf{x}}_{t|t-1} &= \mathbf{F} \hat{\mathbf{x}}_{t-1|t-1}, \\ \mathbf{P}_{t|t-1} &= \mathbf{F} \mathbf{P}_{t-1|t-1} \mathbf{F}^T + \mathbf{Q}, \end{aligned} \quad (11)$$

where $(\cdot)^T$ is the transpose operation.

Upon the reception of the measurement \mathbf{z}_t at time step t , the update stage sequentially determines the innovation $\tilde{\mathbf{y}}_t$, innovation covariance \mathbf{S}_t , optimal Kalman gain \mathbf{K}_t , updated a posteriori state estimate $\hat{\mathbf{x}}_{t|t}$, and updated a posteriori error covariance matrix $\mathbf{P}_{t|t}$ as follows:

$$\begin{aligned} \tilde{\mathbf{y}}_t &= \mathbf{z}_t - \mathbf{H} \hat{\mathbf{x}}_{t|t-1}, \\ \mathbf{S}_t &= \mathbf{R} + \mathbf{H} \mathbf{P}_{t|t-1} \mathbf{H}^T, \\ \mathbf{K}_t &= \mathbf{P}_{t|t-1} \mathbf{H}^T \mathbf{S}_t^{-1}, \\ \hat{\mathbf{x}}_{t|t} &= \hat{\mathbf{x}}_{t|t-1} + \mathbf{K}_t \tilde{\mathbf{y}}_t, \\ \mathbf{P}_{t|t} &= (\mathbf{I} - \mathbf{K}_t \mathbf{H}) \mathbf{P}_{t|t-1} (\mathbf{I} - \mathbf{K}_t \mathbf{H})^T + \mathbf{K}_t \mathbf{R} \mathbf{K}_t^T, \end{aligned} \quad (12)$$

where \mathbf{I} is the identity matrix of size N .

To initialize recursions, we generate an initial rainfall estimate $\hat{x}_{0|0}$ from a multivariate Gaussian distribution with mean μ_0 and covariance matrix $P_{0|0}$. Then rainfall predictions are obtained using Eq. (11). Upon observing the radar reflectivity measurements z_k , we execute the update stage as given in Eq. (12).

4. Numerical results

In this work, we are interested in the precipitations observed in a consecutive 3-day period between 28 November 2016 and 30 November 2016. For 28 November 2016, Figure 3a shows the radar activity over Turkey, where the Çatalca radar is located in the northwest of Turkey. Figure 3b shows the weather activity as radar reflectivity measurements observed by the Çatalca radar. For this 3-day period, the reflectivity values of first-level CAPPI data (within 1 km) are around 30–40 dBZ, and the variability of the reflectivity values is smooth. There are not many peaks above 40 dBZ and rain rates do not exceed 10 mm/h, which can be classified as stratiform precipitation based on the definitions given in Section 2. On the other hand, the presence of a cold-front line with warm air causes rain showers at the beginning of the period, where such showers can be classified as convective precipitation. Both ZR relations for stratiform precipitation and convective precipitation, given in Table 2, are thus considered here for numerical comparison. We refer to ZR relationship $Z = 200R^{1.6}$ as ZR1 (suited for stratiform precipitations) and $Z = 300R^{1.4}$ as ZR2 (suited for convective precipitations).

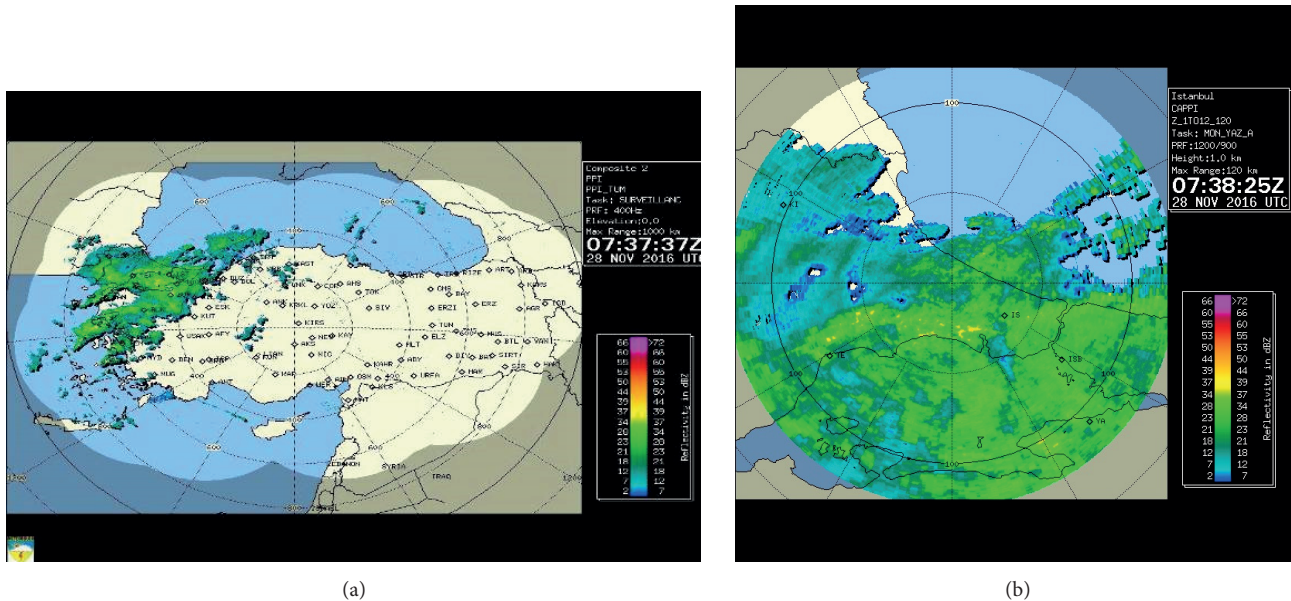


Figure 3. (a) Radar map of Turkey on 28 November 2016, (b) radar reflectivity measurements (in dBZ) within the range of the Çatalca radar.

Let $x_t(n)$ be the actual rainfall measured by the rain gauge sensor of AWOS n at time step t and $\hat{x}_t(n)$ be the estimated rainfall for AWOS n at time step t by using either of the above ZR rules or the Kalman filter. We define the mean squared error (MSE) of the rainfall estimate at AWOS n as

$$\text{MSE}(n) = \frac{1}{T_S} \sum_{t=1}^{T_S} (x_t(n) - \hat{x}_t(n))^2 \quad n \in \{1, \dots, N\}, \quad (13)$$

where T_S is the total number of iterations (time steps) in a 3-day (72-h) period of tracking. Note that

CAPPI provides radar reflectivity measurements every 8 min. Therefore, in order to have a radar reflectivity measurement that can best represent the 1-h weather activity, we select the maximum of the reflectivity measurements observed within the 1-h period. In our study, for our available weather data, we also tried summing all the radar reflectivity measurements, or averaging the reflectivity measurements received in 1 h. When we used the summation of the reflectivity measurements in 1 h and the corresponding rainfall amount in the same hour, the best ZR relationship parameters were obtained as $a = 488.26$ and $b = 1.2512$, which were close to the parameters of a thunderstorm [2]. On the other hand, when we used the average of the reflectivity measurements and the rainfall amount in the same hour, the best ZR relationship parameters were then obtained as $a = 61.0328$ and $b = 1.2512$, which were close to the parameters of a light rain [2]. For our data, the maximum radar reflectivity value in 1 h and the total rainfall amount in the same hour are best modeled with the ZR parameters $a = 158.2116$ and $b = 1.1947$, which are now comparable with the stratiform precipitation parameters ($a = 200$, $b = 1.6$) where our 3-day rainfall data were mostly classified as stratiform.

Then, using either the Kalman filter or empirical ZR relationships, we estimate the rainfall at a particular AWOS location accordingly. The estimated rainfall amount at a given AWOS location is then compared with the actual rainfall amount observed at that location. In this study we initialize the Kalman filter using the ZR1 estimates of the rainfall. For the prediction stage in Eq. (11), the elements of the initial value vector $\hat{x}_{1|1}$ are set as the ZR1 rainfall estimates at each of the AWOS locations. The initial covariance matrix $P_{1|1}$ is set as arbitrary $\sigma^2 I$, where we select $\sigma^2 = 40$ and I represents the identity matrix of size $N \times N$.

For the Kalman filter model, we initially select $N = 5$ AWOSs located at S_1 to S_5 (see Table 3) as shown in Figure 2 and Table 3. The Kalman filter is trained with the first T iterations of actual radar reflectivity and rainfall amount pairs in order to obtain the process/measurement models and covariance matrices of the process noise/measurement noise as defined in Section 3.2. Table 4 shows that for $N = 5$ AWOS locations, the Kalman filter model and empirical ZR relationships achieve similar results in terms of MSE, where the estimation results of the KF converges after about $T = 36$ initial iterations for training. Since the type of precipitation is mostly stratiform, the ZR relationship of the stratiform precipitation (ZR1) yields rainfall estimates with slightly better MSE values as compared to the ZR relationship of the convective precipitation (ZR2).

Table 4. MSE at $N = 5$ AWOS locations as a function of number of training samples T , hourly data.

T	S_1	S_2	S_3	S_4	S_5
24	7.00	2.77	2.01	4.37	3.30
36	2.37	1.06	1.20	1.52	0.57
48	2.34	1.04	1.19	1.48	0.56
60	2.44	1.22	1.30	1.62	0.59
72	2.44	1.23	1.29	1.62	0.60
ZR 1	2.53	1.10	1.33	1.44	0.79
ZR 2	2.89	1.26	1.47	1.64	0.80

To assess the estimation performance of the Kalman filter when the total number of AWOS locations is increased, in Table 5, we set the total number of AWOS locations as $N = 10$ by adding 5 new AWOS locations S_6 to S_{10} (see Table 3). The numerical results in Table 5 show that, when used with $N = 10$ AWOS locations, it is possible to reduce the MSE at S_1 to S_5 as compared to the $N = 5$ case presented in Table 4. When

Table 5. MSE at $N = 10$ AWOS locations as a function of number of samples for training, hourly data; T is the total number of training pairs.

T	S_1	S_2	S_3	S_4	S_5	S_6	S_7	S_8	S_9	S_{10}
24	4.08	2.40	3.90	1.22	1.60	2.32	3.40	5.73	0.94	0.88
36	1.85	0.83	0.88	0.87	0.44	0.74	0.91	1.39	0.23	0.52
48	1.78	0.81	0.87	0.86	0.44	0.72	0.87	1.42	0.23	0.54
60	1.74	0.87	0.85	0.85	0.42	0.69	0.84	1.49	0.21	0.54
72	1.74	0.87	0.85	0.84	0.43	0.70	0.84	1.48	0.20	0.56
ZR1	2.53	1.10	1.33	1.44	0.79	0.88	1.44	1.89	1.85	1.39
ZR2	2.89	1.26	1.47	1.64	0.80	1.03	1.69	1.96	1.44	1.39

Table 6. MSE at $N = 15$ AWOS locations as a function of number of samples for training, hourly data; T is the total number of training pairs.

T	S_1	S_2	S_3	S_4	S_5	S_6	S_7	S_8	S_9	S_{10}	S_{11}	S_{12}	S_{13}	S_{14}	S_{15}
24	10.13	2.32	9.15	15.87	2.67	4.78	5.47	56.35	5.04	1.76	38.59	5.50	5.47	5.79	4.30
36	1.43	0.60	0.62	0.65	0.20	0.47	0.64	1.38	0.15	0.31	0.80	0.91	1.30	0.92	0.36
48	1.03	0.50	0.59	0.64	0.17	0.37	0.56	1.27	0.12	0.26	0.74	0.72	0.94	0.74	0.34
60	0.98	0.46	0.61	0.68	0.17	0.37	0.49	0.84	0.10	0.23	0.76	0.76	0.90	0.75	0.30
72	1.03	0.47	0.61	0.69	0.18	0.38	0.50	0.81	0.10	0.24	0.75	0.80	0.94	0.80	0.31
ZR1	2.53	1.10	1.33	1.44	0.79	0.88	1.44	1.89	1.85	1.39	27.32	2.36	2.12	1.78	1.07
ZR2	2.89	1.26	1.47	1.64	0.80	1.03	1.69	1.96	1.44	1.39	18.21	2.76	2.51	2.05	1.27

used with $N = 10$ AWOS locations, in terms of MSE in estimation, the Kalman filter now outperforms all the ZR relationship-based methods considerably. Furthermore, for $N = 15$ AWOS locations, we further include reflectivity measurements observed from S_{11} to S_{15} (see Table 3). Similar to the previous results, when used with $N = 15$ AWOS locations, the MSEs at S_1 to S_{10} further decrease as compared to the $N = 10$ case presented in Table 5. Finally, we compare the MSE values given in Table 4, Table 5, and Table 6 in terms of the required number of training samples T to fit the Kalman filter model parameters. For all three cases, the MSE of the Kalman filter estimate at a given AWOS location does not change significantly after trained with at least the first $T = 36$ h of data.

Figure 4 shows the amount of actual rainfall and estimated rainfall obtained by either using the ZR1 rule or the Kalman filter at representative S_1 to S_4 AWOS locations over time. When used with $N = 15$ AWOS locations, the Kalman filter rainfall estimation tracks the actual rainfall amounts at each hour better than the Kalman filter as compared to the $N = 5$ case or ZR1 relationship. Finally, Figure 5 shows the minimum achievable MSE at the same AWOS locations, when the number of AWOS locations N in the Kalman filter is varied between 1 and 15. Note that when $N = 1$, the rainfall amount is estimated by using the current and previous reflectivity measurements observed at that AWOS location only, i.e. without using the reflectivity measurements observed at the neighboring AWOS locations. When $N = 1$, the estimation performance of the ZR1 rule is better than the estimation performance of the Kalman filter. This might be due to the fact that ZR relationship parameters (ZR1) have been determined for a statistically very long period of data, where the Kalman filter parameters are obtained in this study by using a very limited number (T) of radar

reflectivity measurement - rainfall amount pairs. As we add reflectivity measurements observed around new AWOS locations, the MSE at the AWOS location of interest tends to decrease. When $N = 5$, ZR1 and the Kalman filter yield similar estimation performances. The estimation performance of the Kalman filter significantly outperforms the estimation performance of ZR1 relationships when N is further increased, i.e. $N = 10$ or $N = 15$.

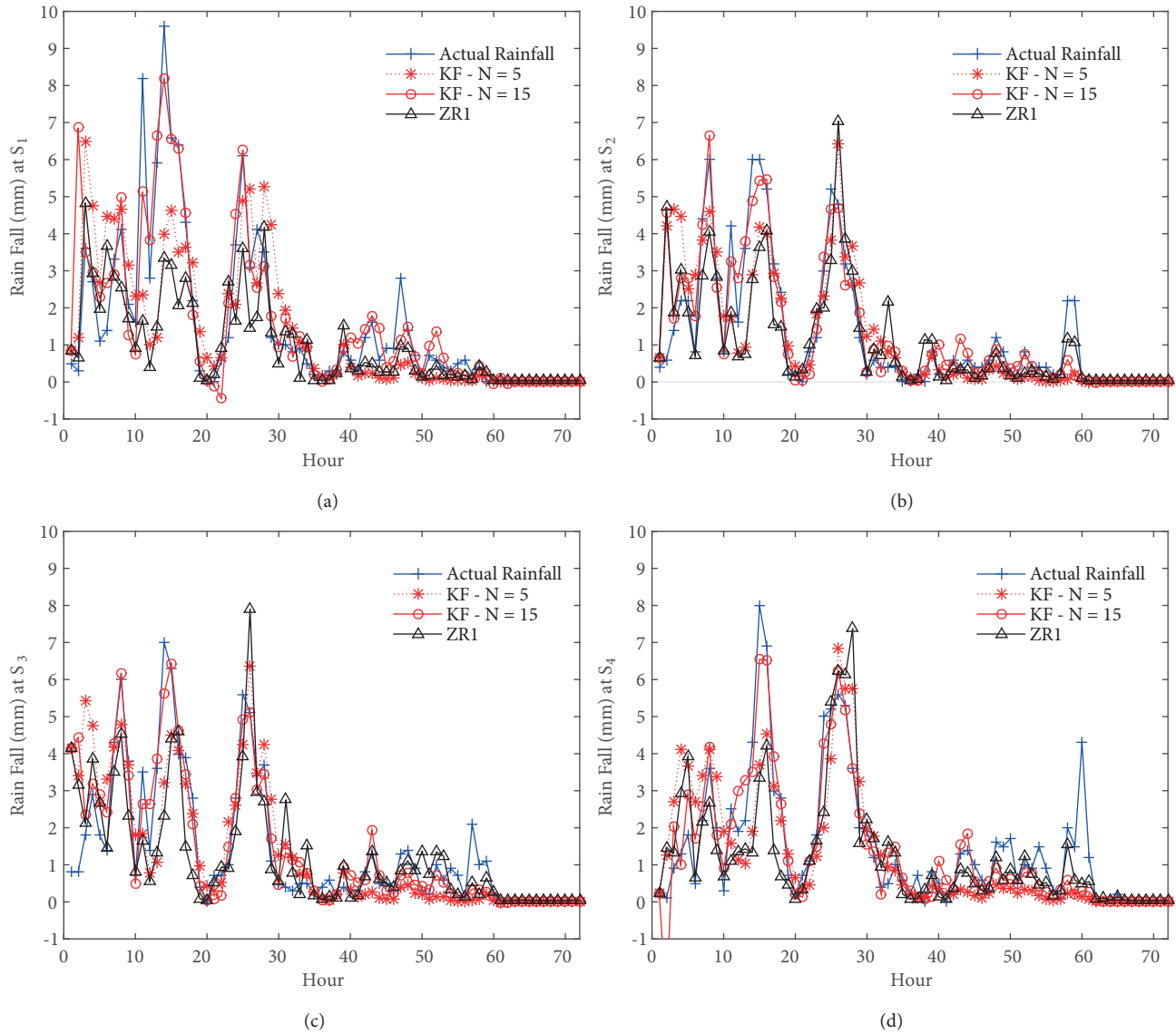


Figure 4. Actual rainfall and estimated rainfall over time observed at (a) S_1 AWOS location, (b) S_2 AWOS location, (c) S_3 AWOS location, and (d) S_4 AWOS location.

5. Conclusions and future work

In this study, we formed a vector Kalman filter whose state vector was composed of true rainfall amounts at N different AWOS locations. The radar reflectivity measurements observed around each AWOS location were then considered as the measurements from the unknown state and the rainfall amounts at the rain gauge sensors of AWOSs were predicted using the Kalman filter. Our preliminary results showed that, for a small number

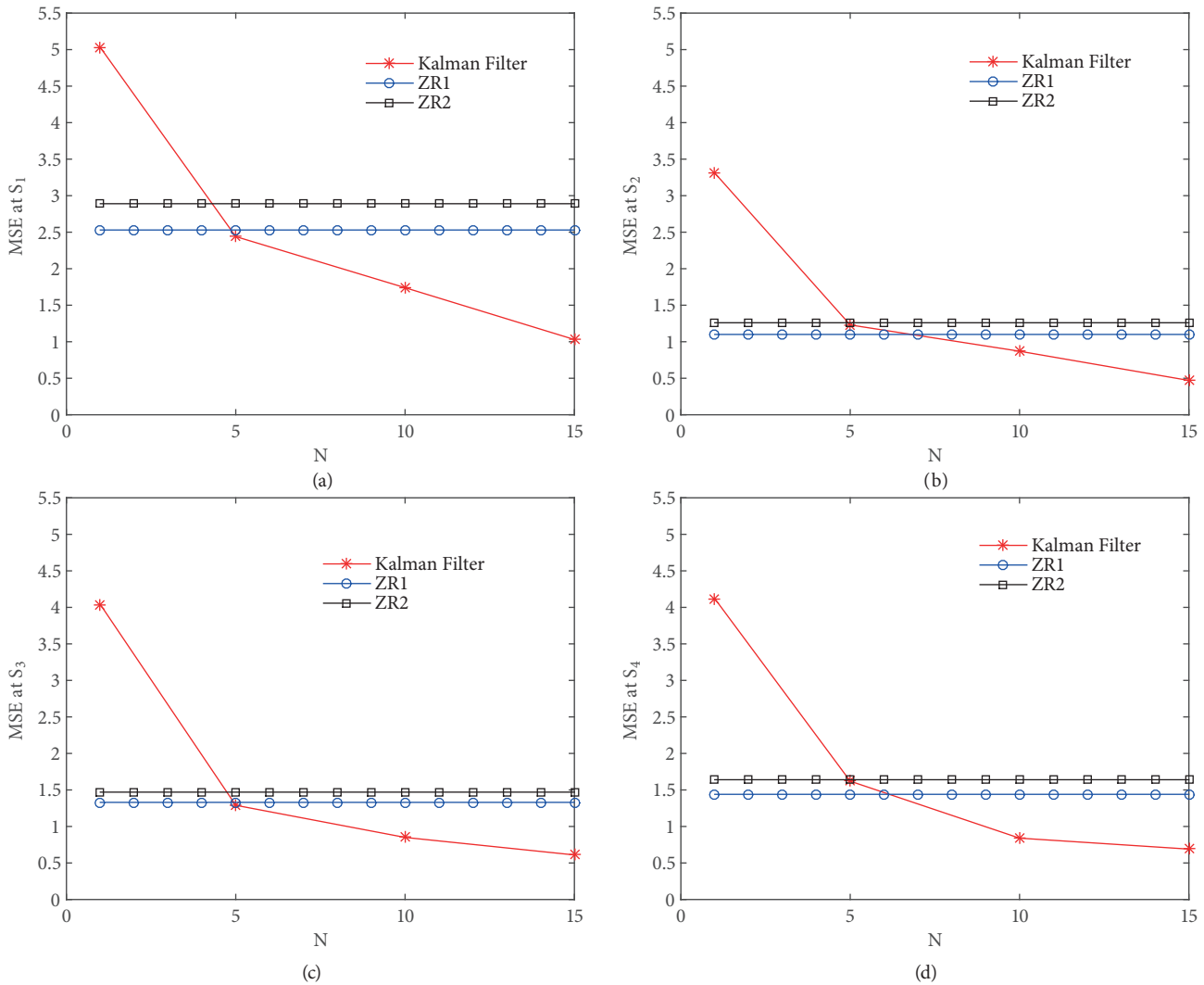


Figure 5. MSE as a function of total number of AWOS locations N observed at (a) S_1 AWOS location, (b) S_2 AWOS location, (c) S_3 AWOS location, and (d) S_4 AWOS location.

of AWOS locations, the empirical ZR model provided better rainfall estimates as compared to the rainfall estimates provided by the Kalman filter. On the other hand, as the number of participating AWOS locations was increased, Kalman filter-based rainfall estimates significantly outperformed the estimates generated with the ZR relationships. As a future work, ZR rule-based rainfall estimates can be integrated into the Kalman filter model as additional measurements. When N is small, the estimation performance of the Kalman filter may thus be improved.

In this study, we compared the performance of the rainfall amount estimation using the Kalman filter with the empirical ZR relationships only. As a future work, we are also interested in determining the estimates by using the spatial and temporal relationship of the rainfall amount data. For this purpose, we need to first select the proper covariance model (or variogram model) of the measurements that can best reflect the spatial and temporal relationship of the rainfall [20, 21], determine the optimal parameters of the covariance model, and compare the estimation results with the ones already obtained in this work.

In this study, we used the maximum of the radar reflectivity measurements observed in a 1-h period to estimate the rainfall amount for that 1-h period. As a future work, the radar reflectivity measurement representing the weather activity in a 1-h period may be improved by using additional radar signal processing. In this study, we consider a stratiform precipitation observed during late November, which was effective over a wide geographical region. The performance of different types of precipitations, i.e. stratiform precipitation or convective precipitation over different time periods within a year, will be studied in detail. Furthermore, we tested our hypothesis with a short period (3-day) of data observed in İstanbul, Turkey. By considering further weather data that span different rain characteristics over different time periods and different regions, we can determine how Kalman filter model parameters depend on the rain type, time of year, and geographical region. If model parameters obtained in one certain region or time period are applicable to other regions or time periods, the need for training the Kalman filter may diminish.

Also in this study, we used the radar reflectivity measurements obtained from a single radar. Fusing radar reflectivity measurements from multiple weather radars may improve the rainfall amount predictions. Moreover, in this work we were interested in the reflectivity data obtained from an altitude of 1 km where CAPPI is capable to get reflectivity values between 1 km and 12 km. Including the reflectivity values obtained from other altitude levels [22] may also improve the rainfall predictions. Last but not least, including data from other sensors, such as temperature, humidity, pressure, wind speed, and wind direction, into the proposed Kalman filter framework may provide very intuitive results to better understand the type and behavior of the precipitation.

Acknowledgment

The authors would like to thank the Turkish State Meteorological Service for providing the weather data.

References

- [1] Fabry F. Radar Meteorology: Principles and Practice. 1st ed. Cambridge, UK, Cambridge University Press; 2015.
- [2] Hazer A, Kara N. Meteoroloji radar agında, ZR iliskisindeki a ve b katsayılarının bulunması ve bunların radara uygulanarak sonuclarin yer gozlemiyle karsilastırılması. In: MGM, III. Meteorolojik Uzaktan Algılama Sempozyumu. Antalya, T urkiye; 16 - 19 Ekim 2017.
- [3] Battan L. Radar observation of the atmosphere. Chicago, USA, The University of Chicago Press. 1973;3:24.
- [4] Dhiram K, Wang Z. Evaluation on radar reflectivity-rainfall rate (ZR) relationships for Guyana. Atmospheric and Climate Sciences. 2016;6(04):489.
- [5] Chumchean S, Sharma A, Seed A. Radar rainfall error variance and its impact on radar rainfall calibration. Physics and Chemistry of the Earth, Parts A/B/C. 2003;28(1-3):27–39.
- [6] Mapiam PP, Sharma A, Sriwongsitanon N. Defining the Z–R relationship using gauge rainfall with coarse temporal resolution: implications for flood forecasting. Journal of Hydrologic Engineering. 2014;19(8):04014003.
- [7] Ruzanski E, Chandrasekar V. Weather radar data interpolation using a Kernel-based Lagrangian nowcasting technique. IEEE Transactions on Geoscience and Remote Sensing. 2015 June;53(6):3073–3083.
- [8] Chumchean S, Seed A, Sharma A. Correcting of real-time radar rainfall bias using a Kalman filtering approach. Journal of Hydrology. 2006;317(1):123 – 137.
- [9] Chumchean S, Sharma A, Seed A. An integrated approach to error correction for real-time radar-rainfall estimation. Journal of Atmospheric and Oceanic Technology. 2006;23(1):67–79.

- [10] Kay SM. Fundamentals of statistical signal processing, Vol. I: Estimation Theory. 1st ed. Upper Saddle River, NJ, USA, Prentice Hall; 1993.
- [11] Costa MAS, Monteiro MSV, Manuela Goncalves A. Kalman filtering approach in the calibration of radar rainfall data: a comparative analysis of state space representations. *Rainfall: Behavior, Forecasting and Distribution*. 2012;p. 167–184.
- [12] Yuehong S, Wanchang Z, Yonghe L, Jingying Z. Analysis of quantitative estimation of precipitation using different algorithms with Doppler radar data. In: 2008 International Workshop on Education Technology and Training 2008 International Workshop on Geoscience and Remote Sensing. vol. 2; 2008. p. 372–375.
- [13] Hamilton JD. Time series analysis. 1st ed. Princeton, NJ, USA, Princeton University Press; 1994.
- [14] Marshall JS, Palmer WMK. The distribution of raindrops with size. *Journal of meteorology*. 1948;5(4):165–166.
- [15] Biggerstaff MI, Listemaa SA. An improved scheme for convective/stratiform echo classification using radar reflectivity. *Journal of applied meteorology*. 2000;39(12):2129–2150.
- [16] Crosson WL, Duchon CE, Raghavan R, Goodman SJ. Assessment of rainfall estimates using a standard ZR relationship and the probability matching method applied to composite radar data in central Florida. *Journal of Applied Meteorology*. 1996;35(8):1203–1219.
- [17] Houze Jr RA. Stratiform precipitation in regions of convection: A meteorological paradox? *Bulletin of the American Meteorological Society*. 1997;78(10):2179–2196.
- [18] Lang S, Tao W, Simpson J, Ferrier B. Modeling of convective–stratiform precipitation processes: sensitivity to partitioning methods. *Journal of Applied Meteorology*. 2003;42(4):505–527.
- [19] Ozturk K, Cubuk A. Orta olcekli konvektif hadiselerde meteoroloji radarlarinin yagis tahminlerinin analizi. In: MGM, III. Meteorolojik Uzaktan Algilama Sempozyumu. Antalya, Turkiye; 16 - 19 Ekim 2017.
- [20] Lichtenstern A. Kriging methods in spatial statistics, Bachelor Thesis, Technische Universitat Munchen. 2013.
- [21] Cressie N, Wikle CK. Statistics for spatio-temporal data. 1st ed. NY, USA, John Wiley & Sons; 2015.
- [22] Tan H, Chandrasekar V, Chen H. A machine learning model for radar rainfall estimation based on gauge observations. In: 2017 United States National Committee of URSI National Radio Science Meeting (USNC-URSI NRSM); 2017. p. 1–2.